Chapter-4

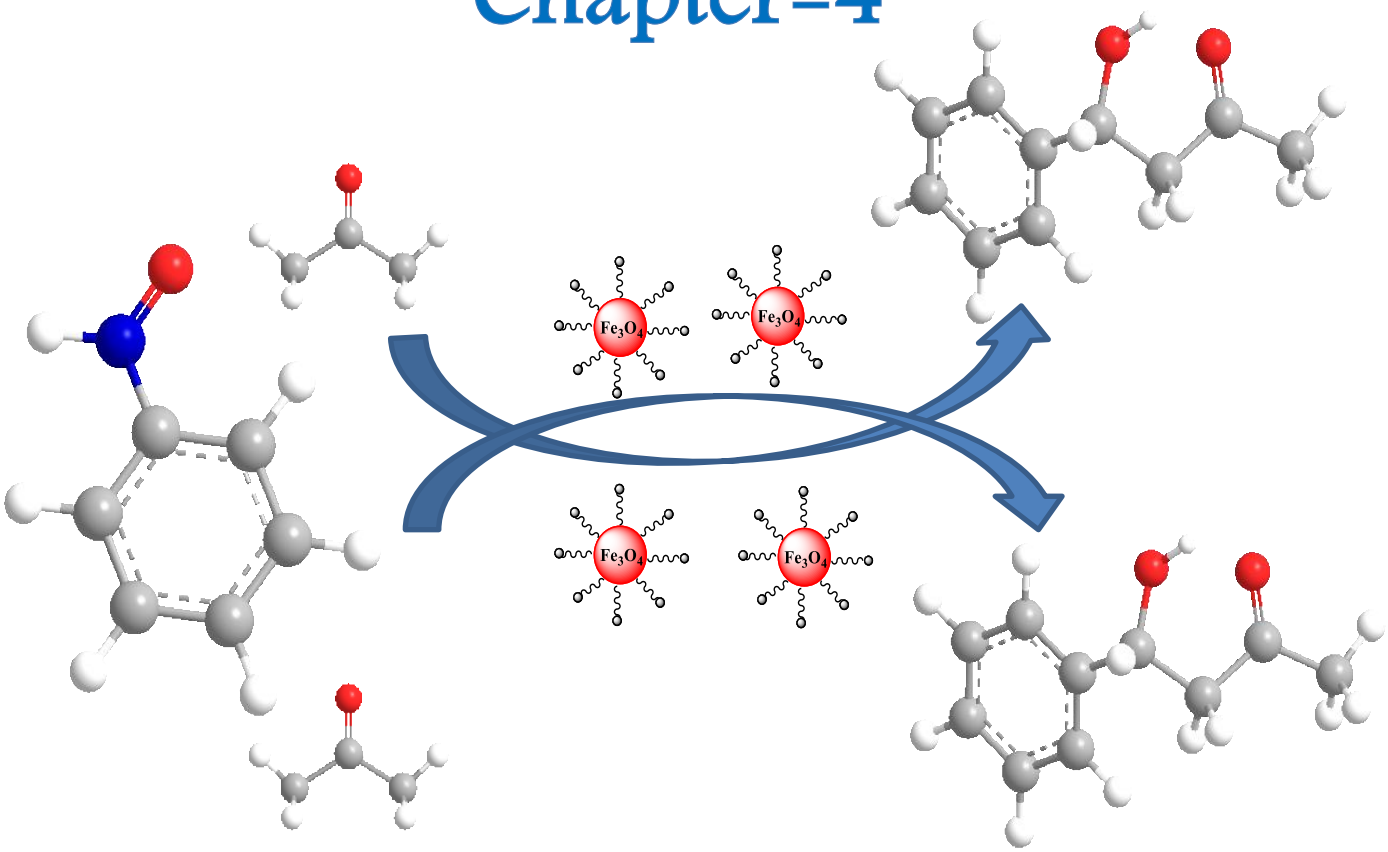

Nanoparticle-supported and magnetically recoverable L-DOPA: Novel catalyst for the room temperature aldol reaction

4.1 Introduction

Hybrid nanoscale materials are well established in various bioprocesses such as nucleic acid detachment,[1] protein separation,[2] immobilization of enzymes[3] and organocatalysis.[4] This environmentally benign approach has been made even greener by grafting the organocatalysts onto solid supports.[5] The aldol reaction is one of the most significant methods to form a carbon–carbon bond in synthetic chemistry.[6] Generally, this reaction catalysed by homogeneous acid or basic solutions through carbocation or carbanion mechanisms.[7] In recent years, several aldol reactions using acid or base catalysts have been reported,[8] including proline-loaded catalysts for stereoselectivity,[9] aldol-type reactions of lithium enolate,[10] iron-catalyzed cross-aldol reactions,[11] and silylenolate.[12] The reaction mechanisms of heterogeneous catalysts are similar to those in homogeneous systems, i.e. definite acidic or basic species must be incorporated onto the catalysts for successful aldol reactions.

The use of primary amines as catalysts in organic reactions is well known in literature.[13] The first primary amine-promoted process was reported more than a century ago.[14] In particular, asymmetric organocatalytic, proline and its various structural derivatives have been shown to be versatile organic catalysts for the intermolecular aldol reactions.[15] Recently, in this context, number of primary amino acids and their derivatives has been shown to act as efficient organocatalysts in enantioselective aldol reactions.[16] Co´rdova et al.[17] demonstrated that linear amino acids such as, alanine can be catalysts for the direct asymmetric intermolecular aldol reaction with excellent stereoselectivity. The process furnished the corresponding β-hydroxy ketones in high yield with upto 99% ee. Surprising, only homogeneous primary amino acids and their structural analogues have been intensively investigated in organocatalytic reactions in the past few years, while the potential of magnetically separable amino acids as organocatalysts was less reported. It is reported, hydrogen bond catalysis at the solid–liquid interface on metal oxide or metal hydroxide nanoparticles for several coupling reactions through solid–liquid interfacial hydrogen bond catalysis.[18] Song et al.[18b] reported, that aldol reactions can be catalyzed by the hydroxyl groups on the $Fe(OH)_3$ shell from Fe_3O_4@$Fe(OH)_3$ core–shell composite

microspheres. This core–shell composite material shows high catalytic activity and the magnetic core makes it recyclable catalyst.

It has been reported that catechol-derived ligands forms a stable, robust anchor on the surface of iron oxide to immobilize functional molecules to the magnetic nanoparticles.[19] Functionalised catechol-derived ligands have been used as agents for the masking of super paramagnetic iron-oxide particles, often so as to render them biocompatible with medium to long-term colloidal stability in the complex chemical environments.[20] Primary amino acids on Fe_3O_4 nanoparticles have demonstrated the power and potential of primary amino group-mediated organic catalysis.

In earlier experiments we observed that the magnetic nanocatalyst shows high catalytic activity and the magnetic core makes it easy to recycle from the reaction mixture.[21] Encouraged by these results, we decided to use Fe_3O_4@L-3,4-dihydroxy phenylalanine (Fe_3O_4@LD) nanocatalyst for aldol reaction. Initially *p*-nitrobenzaldehyde (*p*-NBA) with neat acetone was used as the model system to simplify the analysis and to accelerate the screening speed. Consequently the optimized conditions were used for the synthesis of various β-hydroxy ketones.

4.2 Experimental

4.2.1 Materials

Benzaldehyde, other aldehydes, Acetone, $FeCl_3 \cdot 6H_2O$, $FeCl_2 \cdot 4H_2O$, Ammonium hydroxide, Methanol, Ethanol, DMSO, DMF, Toluene, DME, DCM, Dioxane, $CHCl_3$ and L-3,4-dihydroxyphenylalanine (LD) were purchased from Merck Mumbai, India. All the solutions were prepared using double-distilled and demineralized water.

4.2.2 Synthesis of magnetic nano-ferrites

Fe_3O_4 nanoparticles were synthesized by a co-precipitation method as reported previously.[22] $FeCl_3 \cdot 6H_2O$ (6.95 g) and $FeCl_2.4H_2O$ (10 g) were dissolved in 50 mL of deionized water and stirred at 50 °C for 30 min under a nitrogen atmosphere. Then, ammonium hydroxide (25 %) was added slowly to adjust the pH of the solution to 10. The reaction mixture was then continually stirred for 1 h at 60°C. The nanoparticles were

separated magnetically, washed with water until the pH reached 7, and then dried under vacuum at 60 °C for 2 h. This magnetic nanoferrite (Fe_3O_4) was then used for further chemical modification.

4.2.3 Surface modification of nano-ferrites

Nano-Fe_3O_4 (1 gm) was dispersed in 10 mL water by sonication for 30 min. L-3,4-dihydroxyphenylalanine (1 gm) dissolved in 5 mL of water was added to this solution and again sonicated for 2 h. The amino acid functionalized nanomaterial was then isolated by external magnet, washed with water and dried under vacuum at 60° C for 2 h.

4.2.4 Details of Experimental Procedure for Fe_3O_4-LD Catalysed Aldol reactions

In a typical reaction 4-nitrobenzaldehyde (*p*-NBA) 151mg (1mmol) was used as a starting material. Acetone was used (2 mL) as reactant as well as solvent and Fe_3O_4@LD **(7**0 mg) as a nanocatalyst. All the components were mixed together in 10 mL round bottom flask and the reaction was carried out at room temperature (rt, 25-30 °C) under stirring for 12h. Reaction monitoring was done by thin-layer chromatography (TLC). After completion of the reaction, catalyst was separated magnetically. The product was isolated by evaporation of solvent followed by column chromatography over silica gel (20:80, ethyl acetate in hexane v/v) to provide pure 4-Hydroxy-4-(4-nitrophenyl)butan-2-one in 90±2 % yield. The spectroscopic data of compounds are in good agreement with those reported. The reaction was also carried out with LD, Fe_3O_4 NPs and without catalyst for comparison.

Aldol reaction of other aromatic benzaldehydes with acetone was carried out in a similar manner. The products purified by short-path chromatography (0-30% ethyl acetate in hexane v/v) were analyzed by ^{1}HNMR.

All experiments have been repeated three times and the reproducibility confirmed. The recyclability of the NPs was also surveyed. The NPs were recovered by magnet and washed with water followed by acetone. They were dried at 50 ºC under vacuum and used for the next cycle.

4.2.5 Characterizations methods

The powered X-ray diffraction (XRD) patterns were recorded with a PanAlytical (model; Empyrean) 'X'PERT-PRO XRPD of Cu Kα radiation (λ= 0.15406 nm) on advance X-ray power diffractometer. Samples were prepared by pressing dried powder and patterns were collected with scanning rate of 2°/min and 2θ ranging from 0 to 80°. Surface area and porosity of the nanocatalyst were measured by a volumetric adsorption system (Micromeritics Instrument corporation, USA, model ASAP 2010) using N_2 adsorption/desorption isotherms at 77 K upto 1 bar. Prior to the measurements, the samples were activated (degassed) by heating at the rate of 1 K/min upto 383 K under vacuum. The temperature as well as vacuum was maintained for 7 hours prior to the measurements. Surface area was calculated by Brunauer-Emmet-Teller (BET) method while the porosity by Barrett-Joyner-Halenda (BJH) method. High-Resolution Transmission Electron Microscopy (HR-TEM) was carried out using Jeol (Jem-2100) electron microscope operated at an acceleration voltage of 200 kV. For this purpose, dry powered sample was dispersed in methanol and ultrasonication treatment was given for 30 min. After that sample was deposited onto a carbon-coated grid at room temperature and it was allowed for air-drying (about 6 hours). Selected area electron diffraction patterns (SAED) and Energy-dispersive X-ray spectroscopy (EDX/EDS) were also investigated from the electron micrographs. FT-IR spectra were recorded as KBr pellet on Perkin Elmer RX1 model in the range of 4000-400 cm^{-1}. Magnetic measurements were done by a vibrating sample magnetometer (EG&G Model 155 VSM) at room temperature in the range +20,000 to −20,000 G.

Fe_3O_4-LD nanocatlyst catalyzed aldol reaction was monitored on thin-layer chromatography (TLC). All products of the aldol reaction are commercially available and were identified by comparing their physical and spectral data (m.p., TLC (silica gel 60 F254, Merck, Mumbai, India), and ^1H NMR (BRUKER 400 MHz) with those of authentic samples or reported data.

4.3 Results and Discussions

4.3.1 Catalyst characterization

The magnetite nanoparticles (Fe_3O_4) were prepared by the co-precipitation method.[22] It was reacted with L-3,4-dihydroxyphenylalanine (LD) in water to yield amino acid grafted magnetically recoverable nanoparticles (Fe_3O_4-LD) (**Scheme 4.1**).

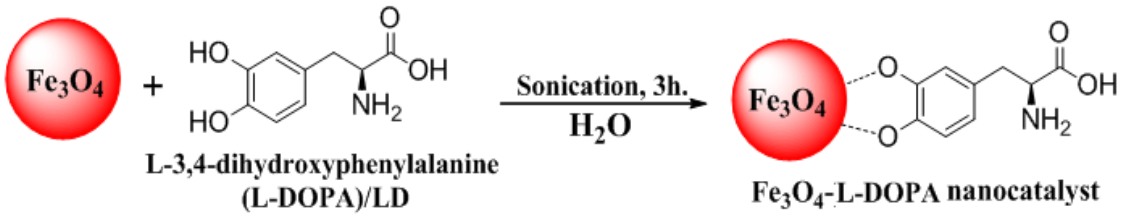

Scheme 4.1 Schematic representation of synthesis of Fe_3O_4-LD nanocatalyst

The High-Resolution Transmission Electron Microscopy (HR-TEM) images of Fe_3O_4-LD nanocatalyst are showing slightly spherical morphology with some cubic partials an average size range of 10–30 nm (**Figure 4.1A**). **Figure 4.1B** and **C** are HR-TEM images of typical Fe_3O_4-LD at different magnifications. The nanoparticles, depicted in **Figure 4.1D** have a discrete core/shell structure, and their uniform magnetic core with a diameter of 10–15 nm is surrounded by a 2–3 nm thick LD organic shell. The high resolution images in **Figure 4.1E** shows well developed lattice fringes and the fringes extend throughout the particle confirming the monocrystalline nature of the individual particles. The distance between adjacent lattice fringes measured as 0.227nm in **Figure 4.1E** corresponds to the 311 reflection. The selected area electron diffraction (SAED) pattern shown in **Figure 4.1F** corresponds to the higher order reflections of Fe_3O_4-LD nanocatalyst. The white spots as well as the bright diffraction rings indicate that the nanoparticles produced by the above stated method are highly crystalline.

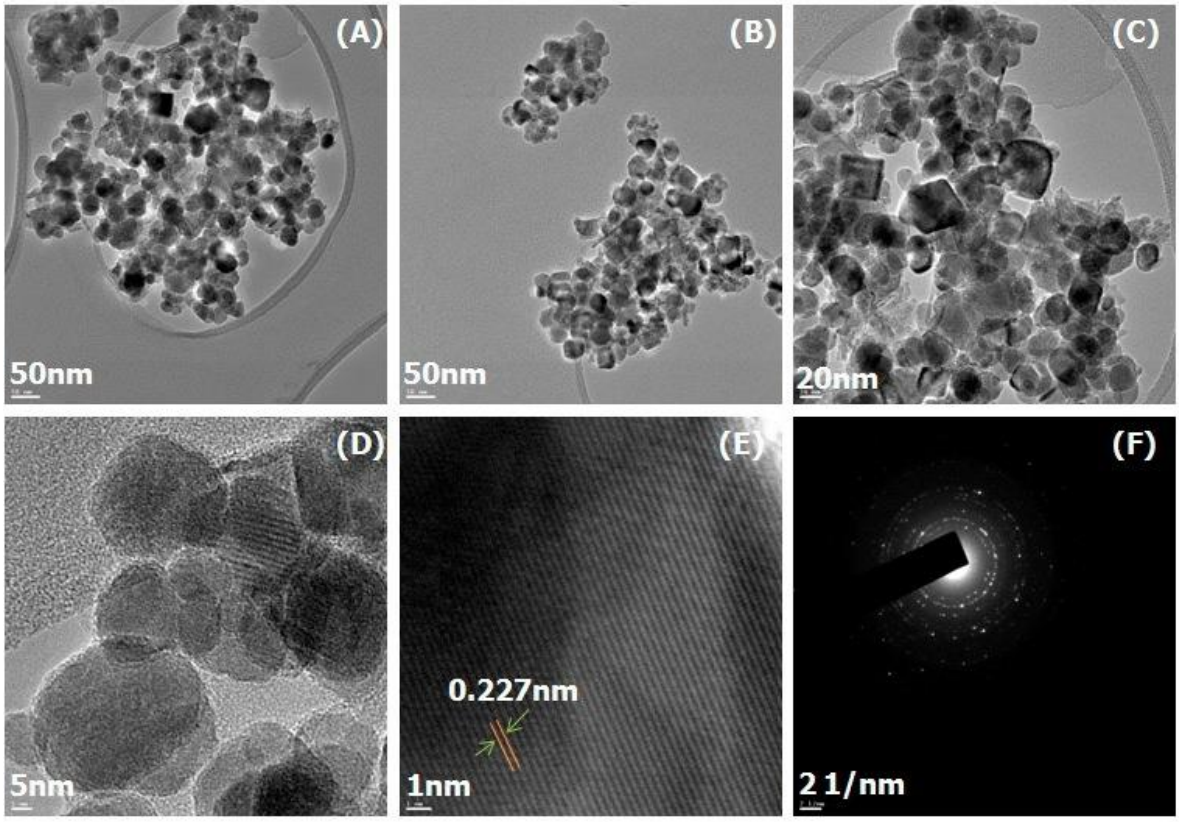

Figure 4.1 HR-TEM images of magnetic Fe_3O_4-LD nanocatalyst at different magnifications (A) 50nm (B) 50nm (C) 20nm and (D) 5nm showing particle size distribution; The resolved lattice fringes and SAED pattern of Fe_3O_4-LD are (E) and (F) respectively.

The crystalline structures of Fe_3O_4 and Fe_3O_4-LD were analysed by powder X-ray diffraction (XRD). As showed in **Figure 4.2A** and **B**, all the samples show diffraction peaks at around 30.1°, 35.2°, 43.1°, 53.5°, 57.4° and 62.7° 2θ corresponding to the spinel structure of Fe_3O_4,[23,28] and which can be assigned to the diffractions of the (220), (311), (400), (422), (511) and (440) faces of the crystals, respectively. The relative intensities of the diffraction peaks matched well with the standard XRD data of Joint Committee on Powder Diffraction Standards (JCPDS) card number (19-0629) for Fe_3O_4 crystal as with a spinel structure, which is consistent with the TEM results. In addition, the XRD patterns depict similar diffraction peaks which indicate that the nanocomposite was

synthesized without damaging the crystal structure of the Fe_3O_4 core. In addition, the broad diffraction peak in the range of 2θ between 10° and 30° can be attributed to the amorphous material coated on the magnetic nanoparticles.[24,29] According to the XRD results, it can be concluded that the Fe_3O_4 nanoparticles were successfully coated with LD. The XRD pattern clearly depicts that there is no change in the topological structure and inherent properties of Fe_3O_4 before and after the coating with LD. On assessment of the diffractograms of LD encapsulated and LD-copper complex grafted nanoparticles, the very distinguishable FCC peaks of magnetite crystal were not changed, which means that these particles have phase stability, but there is a slight decrease in intensity with broadening of the corresponding peak of LD (**Figure 4.2B**). It can be attributed to the lowering of scattering contrast between the walls of the Fe_3O_4 framework and organic moiety attached over Fe_3O_4. It also shows that different reaction conditions during the synthesis, did not affect the crystallinity and morphology of Fe_3O_4 nanoparticles throughout the process.

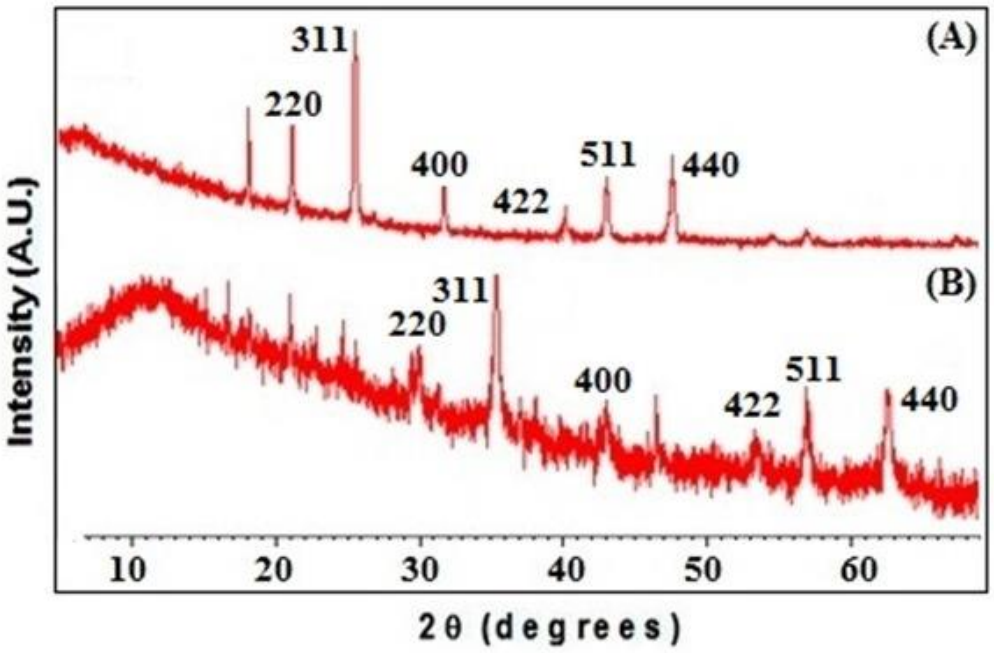

Figure 4.2 XRD pattern of (A) Fe_3O_4 and (B) Fe_3O_4-LD nanocatalyst

Fourier transform infrared spectroscopy (FT-IR) was used for confirmation of the functionalization on magnetic nanoparticles. The FT-IR spectra of the LD and Fe_3O_4 -LD were recorded to confirm the modification of the magnetite surface with the LD (**Figure 4.3A–B**). The IR spectra of LD (**Figure 4.3A**) is showing strong peak around 3404 cm^{-1} due to O–H stretching vibrations of catechol and 1652 cm^{-1} due to C=O stretching of carboxylic acids. The presence of magnetite nanoparticles in Fe_3O_4-LD is observable by the strong absorption band at about 602 cm^{-1}, corresponding to the Fe–O vibrations (**Figure 4.3B**). It is also clear that the strong O–H stretching vibrations of catechol, is generally present at 3400 cm^{-1}, is absent in the spectrum of Fe_3O_4-LD (**Figure 4.3B**). Instead, the broad band around 3106 cm^{-1} due to O–H stretching of carboxylic acids is observed. Compared to LD, Fe_3O_4-LD, exhibits a significant reduction in the intensity of the O–H stretching and bending vibrations bands. The appearance of new bands in the region 463 cm^{-1} can be attributed to the stretching frequency correlated to ν(M–O), which confirmed the coordination through oxygen.[25,30] The FT-IR data confirmed that the L-DOPA was successfully immobilized onto the surface of the magnetic nanoparticles.

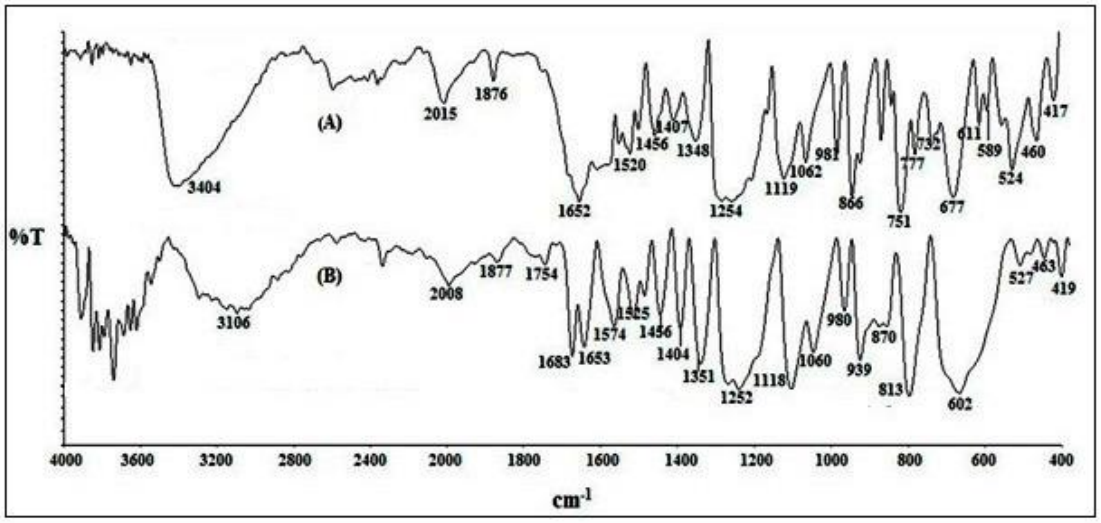

Figure 4.3 FT-IR spectra of (A) LD and (B) Fe_3O_4-LD nanocatalyst

The Energy Dispersive X-ray (EDX) analysis of Fe_3O_4-LD nanocatalyst is indicates that the well-cleaned final product is mostly composed of O, Fe (**Figure 4.4A**) with no other signal in **Figure 4.4A**.

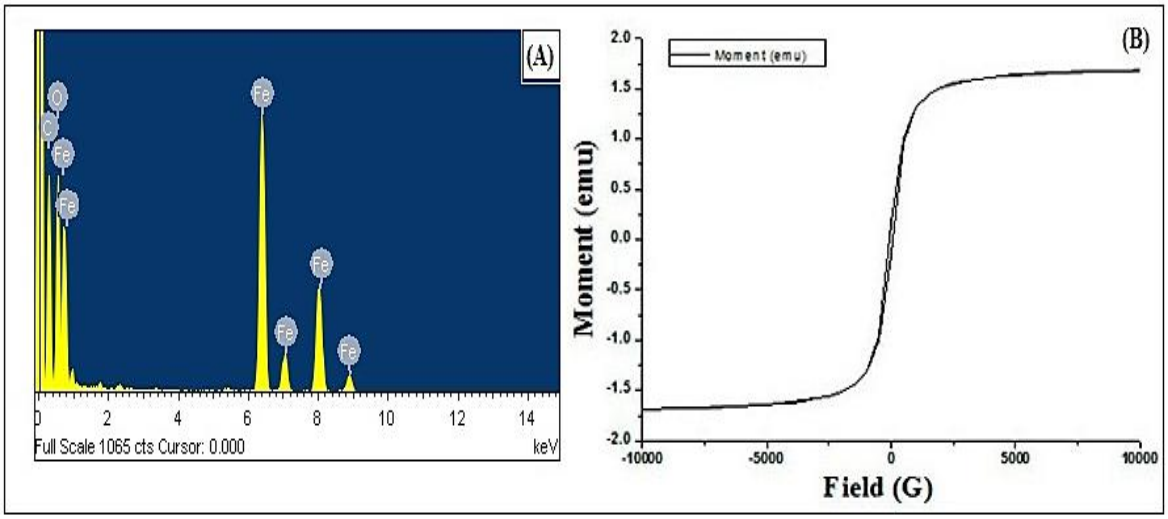

Figure 4.4 (A) EDX patterns and **(B)** Magnetization curves obtained by VSM at room temperature for Fe_3O_4-LD nanocatalyst

The magnetic properties of the synthesized Fe_3O_4-LD were analyzed by vibrating sample magnetometry (VSM). The field-dependent magnetization curves shown in **Figure 4.4B** indicate the magnetization as a function of applied magnetic field, measured at room temperature. The coercivity value of the Fe_3O_4-LD nanoparticles was 73.65. In spite of these low magnetization values with respect to magnetization of pure Fe_3O_4 nanoparticles,[26,22] which was owing to decrease in the surface moments of the magnetite nanoparticles by diamagnetic LD coating over Fe_3O_4 nanoparticles, it is still sufficient for magnetic separation by a conventional magnet. The above mentioned TEM images also confirmed the encapsulation and grafting of the organic layer over Fe_3O_4 nanoparticles. The hysteresis loops of powdered materials showed almost negligible magnetic hysteresis with both the magnetization and demagnetization curves passing through the origin. Thus clearly indicates the super paramagnetic nature of the materials. This also means that the

magnetic material can only be aligned under an applied magnetic field but, will not retain any residual magnetism upon removal of the field. Thus, the Fe_3O_4-LD nanoparticles appear to be suitable as a catalyst.

The Brunauer-Emmet-Teller (BET) surface area of a magnetic Fe_3O_4-LD sample was high 136.81 m^2/g, (**Figure 4.5A**). Similarly, the BJH adsorption and desorption cumulative surface area of pores are 133.81 m^2/g and 133.80 m^2/g respectively (**Figure 4.5B, C and D**).

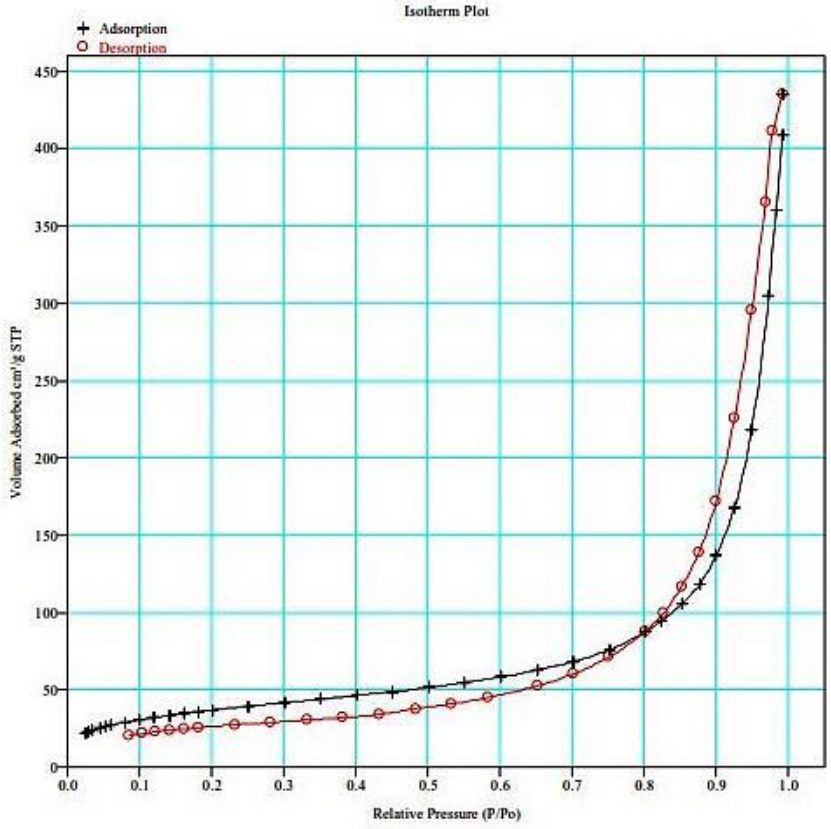

Figure 4.5A BET Isotherm Plot for Fe_3O_4-LD nanocatalyst

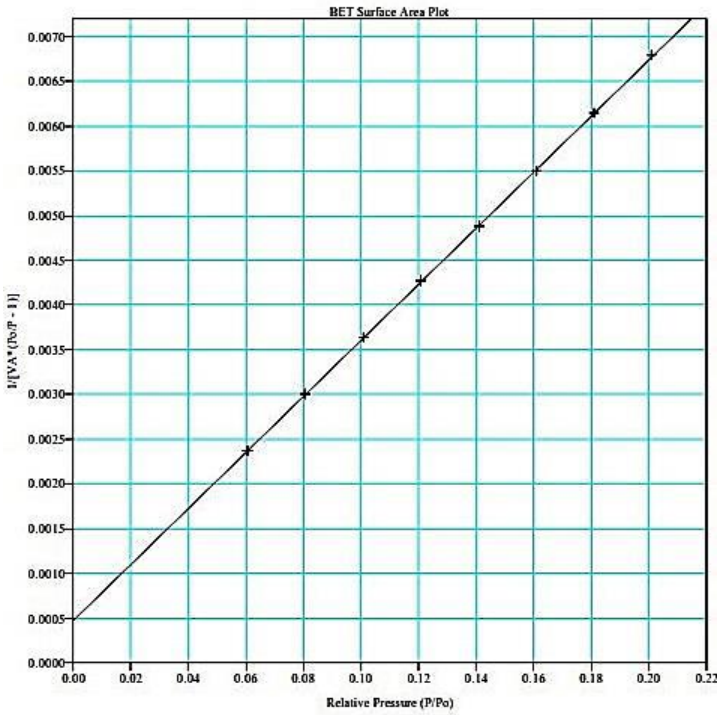

Figure 4.5B BET Surface area Plot for F-e_3O_4-LD nanocatalyst

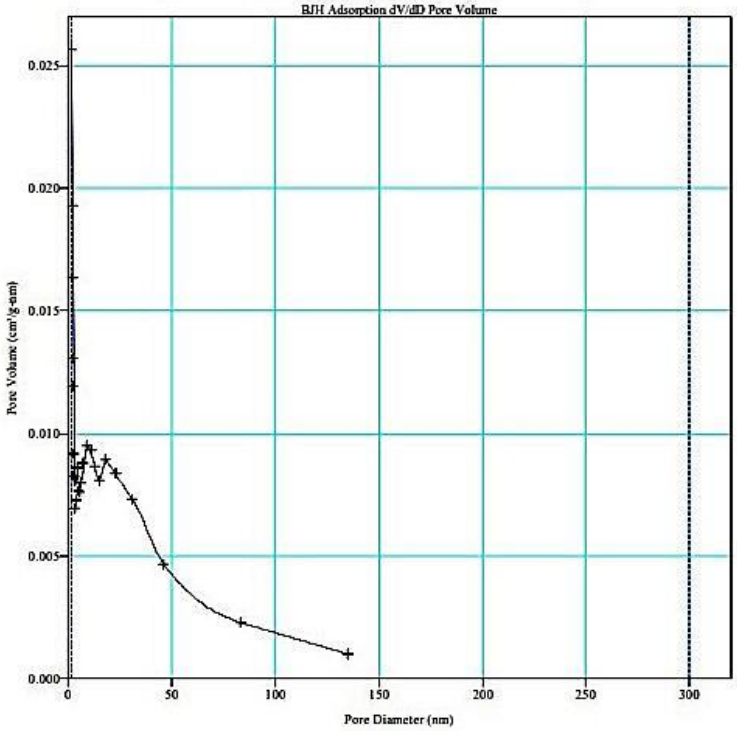

Figure 4.5C BJH Adsorption dV/dD Pore Volume for Fe_3O_4-LD nanocatalyst

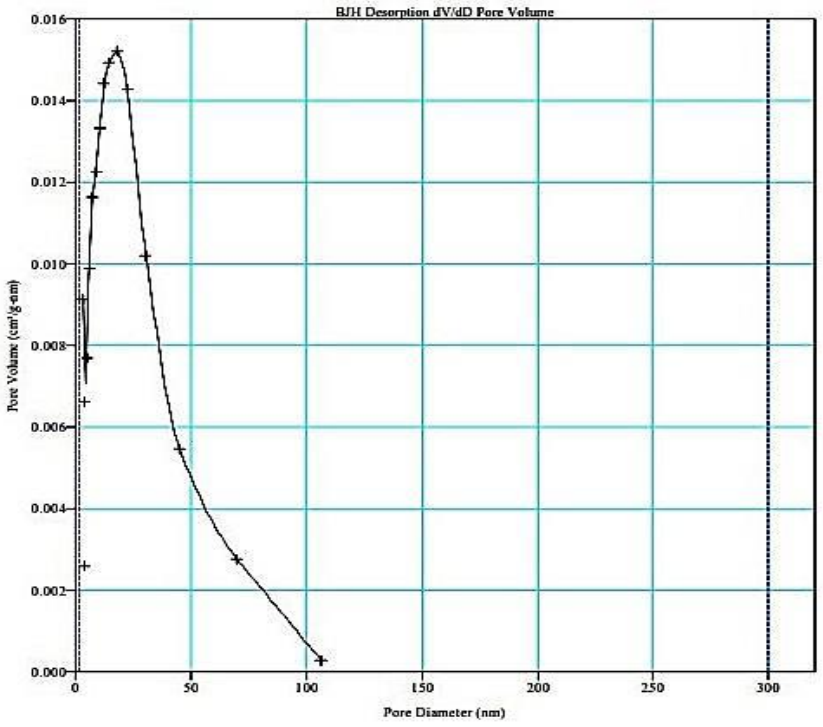

Figure 4.5D BJH Desorption dV/dD Pore Volume for Fe_3O_4-LD nanocatalyst

4.3.2 Catalytic activity

The Fe_3O_4-LD nano-catalyst was employed as heterogeneous catalyst for the aldol reaction of aromatic aldehydes. The aldol reaction was carried out with acetone as solvent as well as reactant. In order to optimize the reaction conditions and obtain the best catalytic activity, the reaction of *p*-nitrobenzaldehyde and acetone was chosen as a model reaction. Different reaction parameters such as solvent, time and amount of catalyst were investigated (**Table 4.1**).

Table 4.1 Effects of different solvent, time and amount of catalyst on the aldol reaction of *p*-nitrobenzaldehyde and acetone in the presence of Fe_3O_4-LD catalyst

Sr. No.	**Catalyst (mg)**	**Solvent**	**Temperature (°C)**	**Time (h)**	**%Yield[b] (±2%)**
1	none	Acetone	25-30	48	-
2	Fe_3O_4[c]	,,	,,	,,	35
3	LD[d]	,,	,,	,,	60
4	50	,,	,,	,,	72
5[a]	**70**	**,,**	**,,**	**12**	**90**
6	90	,,	,,	12	90
7	70	MeOH	,,	16	89
8	70	EtOH	,,	16	87
9	70	DCM	,,	24	61
10	70	DME	,,	24	55
11	70	DMSO	,,	24	47
12	70	DMF	,,	24	33
13	70	Toluene	,,	24	71
14	70	$CHCl_3$	,,	24	41
15	70	Dioxane	,,	24	45
16	70	THF	,,	24	55
17	70	DMSO:Water(8:2)	,,	24	87

The reaction of *p*-nitrobenzaldehyde (1mmol) with acetone (5 mmol) in different solvents (2 mL) was carried out in the presence of a catalyst (70 mg) at room temperature.

a- optimized reaction condition, b- Isolated yield, c-Iron oxide only (70 mg) and d-LD only (70mg).

It is seen from the **Table 4.1** (entry-1) that the presence of a catalyst is required for aldol reaction of *p*-nitrobenzaldehyde and acetone. In order to investigate the role of LD in the catalyst, the model reaction was carried out under the optimized reaction conditions in the presence of Fe_3O_4NPs (**Table 4.1**, entry-2). No progress in the reaction was observed even after 48 h. Thus, it can be concluded that LD incorporated onto the magnetic nanoparticle plays a pivotal role in the solvent-free as well as with solvent promoted aldol reaction of of *p*-nitrobenzaldehyde and acetone. Similar, pure LD as catalyst attended only 60% yield after 48h (**Table 4.1**, entry-3).

It was observed that the best yield and selectivity were obtained when the reaction was conducted under solvent-free conditions (entry-5). Moreover, the effect of the catalyst amount on the aldol reaction was also investigated by varying the amounts of the catalyst (**Table 4.1**, entries 4 and 6). As can be seen, while the amount of catalyst increased from 50 to 70 mg (entries 4 and 5), the product yield increased from 72% to 94%, which is probably due to the availability of more catalytic sites. Since, the percentage yield remained stable between 70 mg to 90 mg catalyst (**Table 4.1**, entries 5 and 6). 70 mg was chosen as the optimum amount of catalyst for the further steps (**Table 4.1**, entry-5, **Scheme 4.2**). As far as the effect of solvent is concerned, the model reaction was performed in several solvents as well as in solvent free conditions (**Table 4.1**, entries-5 to17). Since acetone is appropriate solvent, it was not suitable for the other reaction systems. Thus, seven different solvents were screened (**Table 4.1**, entries 7–17). We found that in alcohol solvents, such as MeOH and EtOH, the process was completed in a longer time but with almost the same yield (**Table 4.1**, entries 7 and 8). When the reaction was performed in DCM, DME, THF, Toluene, DMF, DMSO, $CHCl_3$ or dioxane, the reaction time and yield was slightly inferior to the results obtained in alcohols. In case of DMSO:Water (**Table 4.1**, entrie-17) mixture 87% yield was obtained.

The influence of reaction temperature on the catalytic activity was investigated by several separate reactions under the same reaction conditions. According to the results the reaction temperature of 25-30 °C appears to be the optimum reaction temperature for reaction (**Table 4.1**, **Scheme 4.2**).

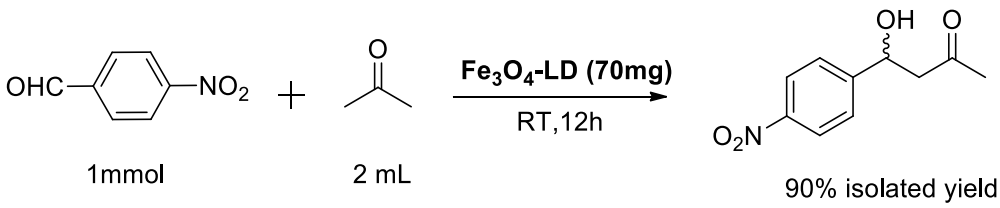

Scheme 4.2 Aldol reaction of *p*-nitrobenzaldehyde and acetone under optimum reaction condition

---

After optimization of the reaction conditions (**Table 4.1**), the catalytic activity of magnetic Fe_3O_4-LD nanocatalyst was further explored, with other aromatic aldehydes. A variety of aromatic aldehydes were tested for the reaction along with acetone as a donor (**Table 4.2, Scheme 4.3**). The Fe_3O_4-LD catalyst exhibited good activity in the solvent-free aldol reaction of different aromatic aldehydes (**Table 4.2**). All the investigated aldehydes with either electron-donating or electron-withdrawing substituents can be transformed to their corresponding aldol adduct in high yields. Further, chiral nature of catalyst opens up new possibilities for enantioselective aldolization processes. High levels of chemical yield (>85%) were observed in electron-poor aldehydes (entries 1–5). Current limitations of the protocol include electron-rich aldehydes, which require a long reaction time and resulted in a low yield (entries 6-7).

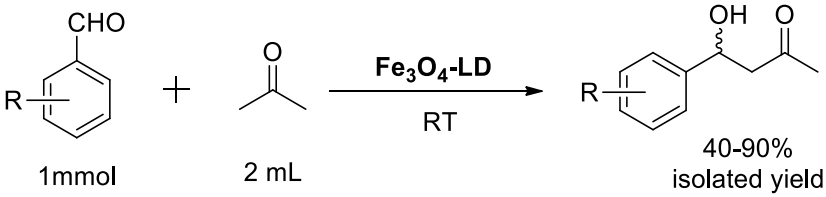

Scheme 4.3 General scheme for Aldol reaction of various aromatics aldehydes and acetone

---

Table 4.2 Aldol reaction of various aromatics aldehydes and acetone over Fe_3O_4-LD nanocatalyst

Entry[a]	Aromatic aldehyde (R-Ph)	Time (h)	Yield[b] (±%)
1	4-NO_2-Ph	12	90
2	3-NO_2-Ph	12	91
3	2-NO_2-Ph	12	89
4	4-CN-Ph	24	79
5	3-F-Ph	24	72
6	4-OH-Ph	24	40
7	4-Cl-Ph	24	67

a- The reaction of aldehyde (1 mmol) with acetone (2mL) was carried out in the presence of 70mg Fe_3O_4-LD nanocatalyst at room temperature for 12–24 h.

b- Isolated yields.

4.3.3 Mechanism investigation

Many studies on the enamine based mechanism under different conditions proposed that L-proline acts as an 'aldolase' type catalyst.[27] Other amino acid like L-Phenylalanine also catalysed direct asymmetric aldol reactions.[28] In the present study, we propose the similar mechanism, however, in this case surface Fe_3O_4 facilitate the catalytic activity of LD by acting as Lewis acids and providing coordination sites for the leaving group.[29] However, the hydroxyl groups on the Fe_3O_4 surface, like the silanol groups on silica, are considered very weak acids, thus it is unlikely that cationic or anionic intermediates are formed in these Fe_3O_4-LD catalyzed reactions, especially considering that these reactions were carried out at room temperature. The weakly acidic surface hydroxyl groups often form hydrogen bonds with oxygenates.[30] While, literature suggests that three possible mechanisms for the primary amino acid catalyzed aldol reactions: 1) the carboxylic acid catalyzed enamine mechanism, 2) the amino catalyzed enamine mechanism, and 3) the enaminium catalysed mechanism. Cordova et al., showed for alanine that the carboxylic acid catalyzed enamine mechanism is more favourable than other mechanisms because it requires the lowest activation energy.[31] On the basis of literature, we proposed a plausible

mechanism in **scheme 4.4**. In the present study, we believe that H-bonds catalyze the aldol reactions and LD favourable to carboxylic acid catalyzed enamine mechanism. As illustrated in the transition state, Fe_3O_4 and carboxylic group of amino acid make H-bonds with the carbonyl group of the aldehyde and prefer to orient in such a way that H-bonding among carbonyl oxygen, Fe_3O_4 coordinated hydroxyl group's surface proton and electron rich $–CH_2$ group is facilitated. The metal core and L-3,4-dihydroxy phenylalanine (LD, amino acid) concomitantly contribute to make the system an effective catalyst.

4.3.4 Recycling of nano-catalyst

The recycling of used catalyst is one of the most important conditions of industrial based catalyst system, which gives useful information about the catalytic stability along the catalytic cycles. The reusability of the catalyst was tested by carrying out repeated runs of the reaction on the same batch of the catalyst in the model reaction (**scheme 4.2**). In order to regenerate the catalyst, after each cycle, it was separated by an external magnet (**Figure 4.6A**; **a and b**) and washed several times with acetone. Then it was dried in an oven at 50 °C and reused in the subsequent run. The results show that this Fe_3O_4-LD magnetic catalyst can be reused five times with no significant loss of activity (**Table 4.3**). It should be mentioned that the catalyst exhibited high stability even after five recycles (**Table 4.3**). After that, however, the reaction time increased with each successive recycling experiment reaching from 12h to 20h (**Table 4.3**). This may be due to gradual loss of the catalytic activity of the nanocatalyst with number of runs due to various reasons. One of the reasons may be surface modification due to deposition of matter during reaction.[32] The HR-TEM images of the nanocatalyst were recorded after 5^{th} run of (**Figure 4.3**) reaction between *p*-nitrobenzaldehyde and acetone. The image in **Figure 4.3B** shows that lattice fringes were damaged by deposited matter throughout the particle. The HR-TEM images display an agglomeration of NPs due to deposited matter (**Figure 4.3 C and D**).

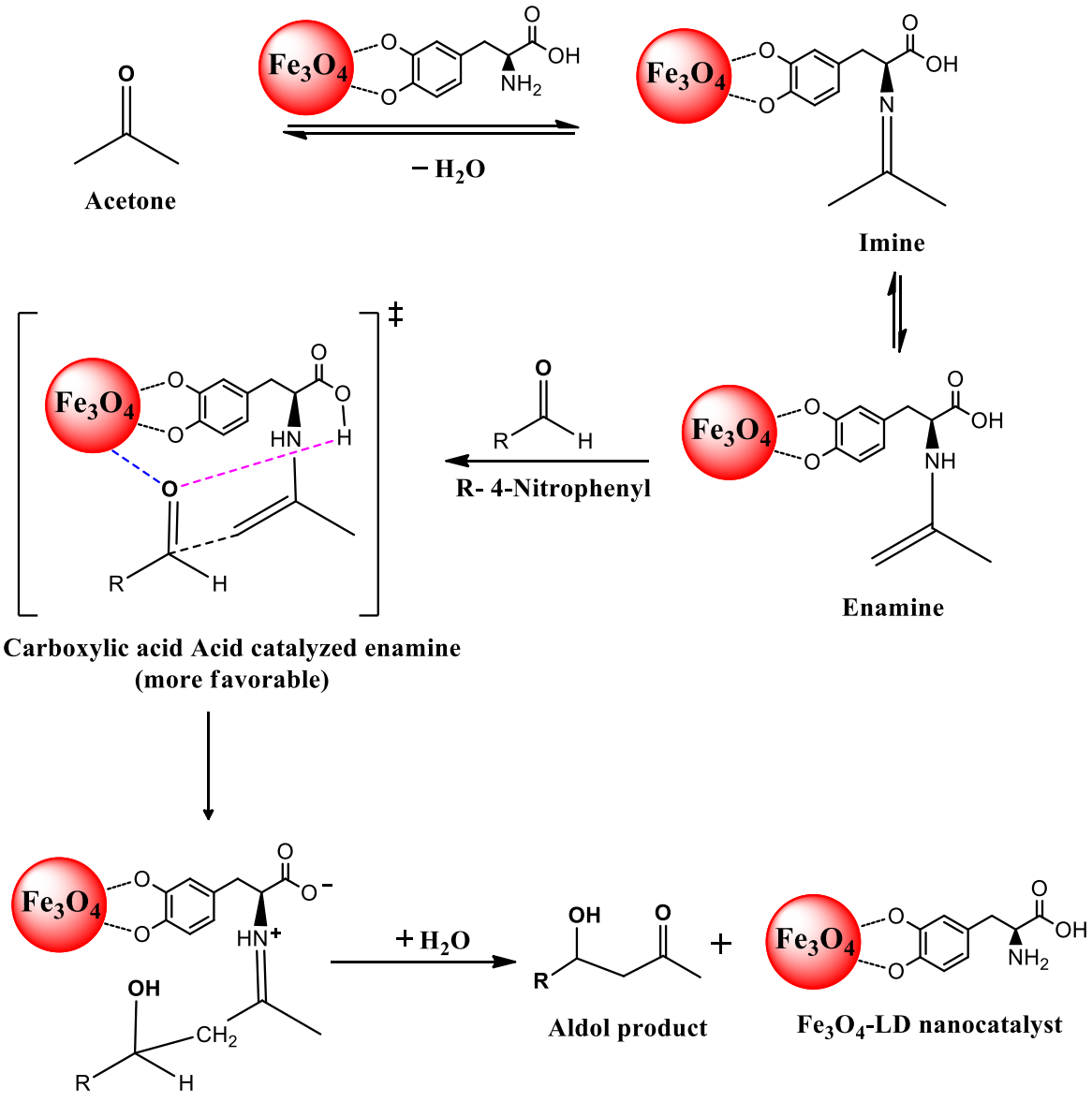

Scheme 4.4 Proposed reaction mechanism showing the mediation of the Fe_3O_4 surface coordinated LD as a magnetic spreadable nanocatalyst for aldol reaction.

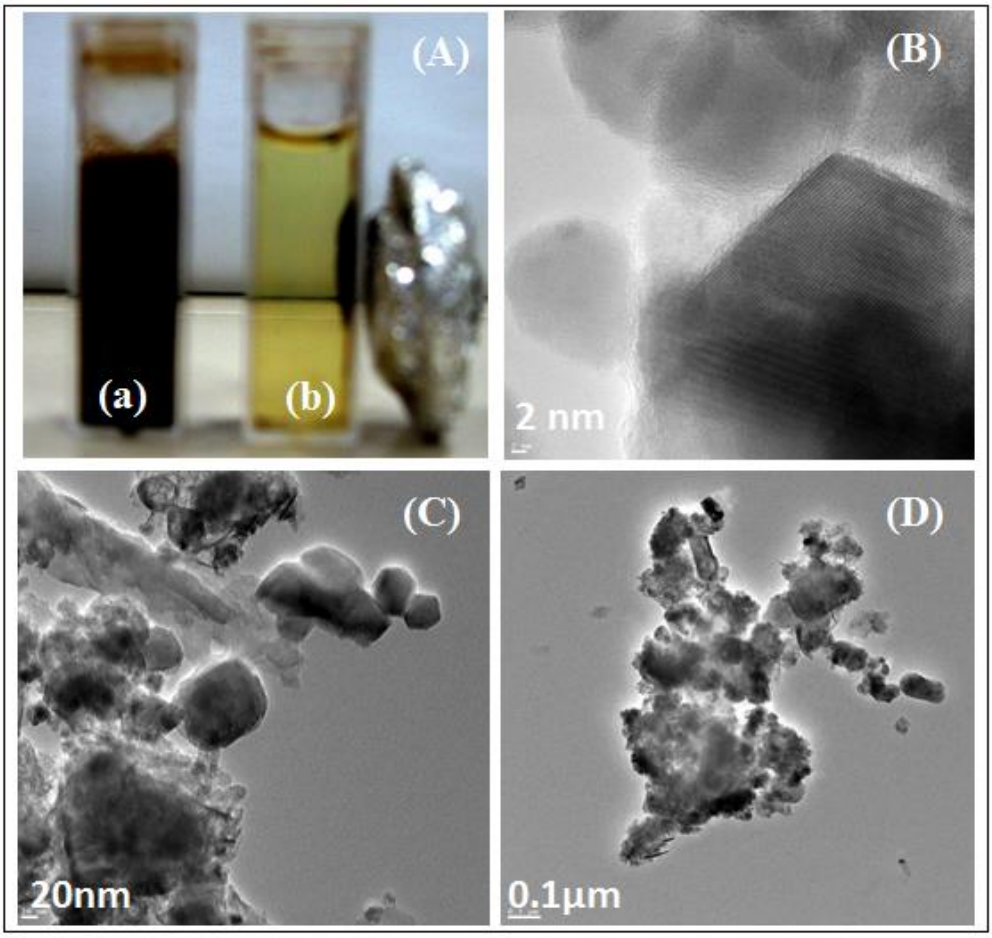

Figure 4.6 (A) Reaction mixture of *p*-nitrobenzaldehyde and acetone (a) before and (b) after magnetic separation by simple magnet; HR-TEM of reused magnetic Fe_3O_4-LD nanoparticles at different magnifications (B) 2 nm (lattice fringes), (C) 20 nm and (C) 0.1µm.

Table 4.3 Recycling experiments of *p*-nitrobenzaldehyde and acetone in the presence of Fe_3O_4-LD catalyst in optimum condition

No. Cycle	**1**	**2**	**3**	**4**	**5**
Time (h)	12	12	13	15	20
Yield (%±2)	90	90	90	88	89

It is evident that the Fe_3O_4-LD nanocatalyst is highly efficient in catalyzing the aldol reaction and gave products in good yields in comparison to the previous literature reports.[33] Hence, catalytic efficiency of the present catalytic system is remarkable in terms of mild reaction conditions, catalyst costs, short reaction time, high reaction yield and easy recovery of the catalyst. Moreover, our catalyst is chiral in nature so this study in future may provide key insights into the origin of magnetic spreadable nanocatalyst for the stereoselective reactions.

4.4 Conclusion

In summary, a facile route to the synthesis of a magnetically separable amino acid for aldol reaction by using Fe_3O_4 and L-3,4-dihydroxyphenylalanine was reported, without using any precursors. This catalyst then catalyzed the aldol reaction with high yield. Also, being magnetically separable, the requirement of catalyst filtration after completion of the reaction was eliminated, which is an additional sustainable quality of this aldol reaction. The magnetic catalyst exhibited high catalytic activity/selectivity in the solvent-free aldol reaction. This study paves the way for further exploration of such catalysts in a broader scope of organic transformations and asymmetric organocatalytsis.

4.5 References

1. P. R. Levison, J. Dennis, S. E. Badger, P. Hathi, M. J. Davis, I. J. Brue and D. Schimkat, *J. Chromatogr., A*,1998, **816**, 107.

2. O. Diettrich, K. Millsa A. W. Johnson, A. Hasilik and B. G. Winchester, *FEBS Lett.*, 1998, **441**, 369.

3. R. F. H. Dekker, *Appl. Biochem. Biotechnol.*, 1989, **22**, 289.

4. (a) A. Dyal, K. Loos, M. Noto, S. W. Chang, C. Spagnoli, K. V. P. M. Shafi, A. Ulman, M. Cowman and R. A. Gross, *J. Am. Chem. Soc.*, 2003, **125**, 1684.

5. (a) T. D. Beeson, A. Mastracchio, J. B. Hong, K. Ashton and D. W. C. MacMillan, *Science*, 2007, **316**, 582;(b) A. Bruckmann, A. Krebs and C. Bolm, *Green Chem.*, 2008, **10**, 1131.

6. (a) R. Mahrwald, Modern Aldol Reactions; Wiley-VCH: Weinheim, 2004;(b) R. Mahrwald, Aldol Reactions; Springer: Heidelberg, 2009.

7. R. Mestres, *Green Chem.*, 2004, **6**, 583.

8. M. L. Kantam, B. M. Choudary, C. V. Reddy, K. K. Rao and F. Figueras, *Chem. Commun.*, 1998, 1033.

9. (a) E. G. Doyaguez, F. Calderon, F. Sanchez and A. Fernandez-Mayoralas, J. *Org. Chem.*, 2007, **72**, 9353; (b) F. Calderon, R. Fernandez, F. Sanchez and A. Fernandez-Mayoralas, *Adv. Synth. Catal.*, 2005, **347**, 1395; (c) M. R. M. Andreae and A. P. Davis, *Tetrahedron: Asymmetry*, 2005, **16**, 2487.

10. Y. Wei and R. Bakthavatchalam, *Tetrahedron Lett.*, 1991, **32**,1535.

11. H.-J. Li, W.-J. Li and Z.-P. Li, *Chem. Commun.*, 2009, 3264.

12. B. C. Ranu and R. Chakraborty, *Tetrahedron*, 1993, **49**, 5333.

13. L-W. Xu, J. Luo and Y. Lu, *Chem. Commun.*, 2009, 1807.

14. (a) E. Knoevenagel, *Ber. Dtsch. Chem. Ges.*, 1894, **27**, 2345; (b) L. F. Tietze and U. Beifuss, in Comprehensive Organic Synthsis, ed. B. M. Trost and Fleming, Pergamon, Oxford, UK, 1991, vol. 2, p. 341.

15. (a) B. List, R. A. Lerner and C. F. Barbas, III, *J. Am. Chem. Soc.*, 2000, **122**, 2395; (b) W. Notz and B. List, *J. Am.Chem. Soc.*, 2000, **122**, 7386; (c) K. S. Sakthivel, W. Notz, T. Bui and C. F. Barbas III, *J. Am. Chem. Soc.*, 2001, **123**, 5260;

(d) B. List, P. Porjarliev and C. Castello, *Org. Lett.*, 2001, **3**, 573; (e)A.Cordova, W. Notz and C. F. Barbas III, *Chem. Commun.*, 2002, 3024; (f) A. Cordova, W. Notz and C. F. Barbas III, *J. Org. Chem.* , 2002, **67**, 301; (g) A. B. Northrup and D. W. C. MacMillan, *J. Am. Chem. Soc.*, 2002, **124**, 6798; (h) A. Bøgevig, N. Kumaragurubaran and K. A. Jørgensen, *Chem. Commun.*, 2002, 620; (i) Z. Tang, F. Jiang, L.-T. Yu, X. Cui, L.-Z. Gong, A.-Q. Mi, Y.-Z. Jiang and Y.-D. Wu, *J. Am. Chem. Soc.*, 2003, **125**, 5262; (j) H. Torii, M. Nakadai, K. Ishihara, S. Saito and H. Yamamoto, *Angew. Chem., Int. Ed.*, 2004, **43**, 1983; (k) A. Hartikka and P. I. Arvidsson, *Tetrahedron: Asymmetry*, 2004, **15**, 1831; (l) A. Berkessel, B. Koch and J. Lex, *Adv. Synth. Catal.*, 2004, **346**, 1141; (m) A. J. A. Cobb, D. M. Shaw, D. A. Longbottom, J. B. Gold and S. V. Ley, *Org. Biomol. Chem.*, 2005, **3**, 84; (n) J. Casas, M. Engqvist, Ibrahem, B. Kaynak and A. Cordova, *Angew. Chem., Int. Ed.*, 2005, **44**, 1343; (o) D. Enders and C. Grondal, *Angew. Chem., Int. Ed.*, 2005, **44**, 1210; (p) I. Ibrahem and A. Cordova, *Tetrahedron Lett.*, 2005, **46**, 3363; (q) A. I. Nyberg, A. Usano and P. Pihko, *Synlett*, 2004, 1891; (r) M. Nakadai, S. Saito and H. Yamamoto, *Tetrahedron*, 2002, **58**, 8167.

16. L-W. Xu and Y. Lu**,** *Org. Biomol. Chem.*, 2008, **6**, 2047.

17. A. Cordova, W. Zou, I. Ibrahem, E. Reyes, M. Engqvist and W-W. Liao, *Chem. Commun.*, 2005, 3586.

18. F. Niu, C.-C. Liu, Z.-M. Cui, J. Zhai, L. Jiang and W.-G. Song, *Chem. Commun.*, 2008, 2803 ;(b) F. Niu, L. Zhang, S-Z. Luo and W-G. Song, *Chem. Commun.*, 2010, **46**, 1109; (c) F. Niu, J. Zhai, L. Jiang and W.-G. Song, *Chem. Commun.*, 2009, 4738.

19. C. J. Xu, K. M. Xu, H. W. Gu, R. K. Zheng, H. Liu, X. X. Zhang, Z. H. Guo, B. Xu, *J. Am. Chem. Soc.*, 2004, **126**, 9938.

20. A. K. L. Yuen, G. A. Hutton, A. F. Masters and T. Maschmeyer, *Dalton Trans*., 2012, **41**, 2545.

21. P. S. Rathore, R. Patidar, T. Shripathi and S. Thakore, *Catal. Sci. Technol.*, 2015, **5**, 286.

22. E. Karaoğlu, A. Baykal, M. Senel, H. Sözeri and M. S. Toprak, *Mater. Res. Bull.*, 2012, **47**, 2480.

23. L. Cabrera, S. Gutierrez, M. P. Morales, N. Menendez and P. Herrasti, *J. Magn. Magn. Mater.*, 2009, **321**, 2115.

24. H. Deng and Z. Lei, *Composites, Part B*, 2013, **54**, 194.

25. H. Mart, *J Macromol Sci, Pure Appl Chem*, 2005, **42**, 1197.

26. F. Zamani, S. M. Hosseini and S. Kianpour, *Dalton Trans.*, 2014, DOI: 10.1039/c3dt52729h

27. (a) B. List, A. L. Richard and C. F. Barbas III, *J. Am. Chem. Soc.*, 2000, **122**, 2395; (b) F. R. Clemente and K. N. Houk, *Angew. Chem., Int. Ed.*, 2004, **43**, 5766; (c) S. Bahmanyar and K. N. Houk, *J. Am. Chem. Soc.*, 2001, **123**, 11273; (c) E. Shah and H. P. Soni, *RSC Adv.*, 2013, **3**, 17453.

28. Z. Jiang, H. Yang, X. Han, J. Luo, M. W. Wong and Y. Lu, *Org. Biomol. Chem.*, 2010, **8**, 1368.

29. F. Niu, L. Zhang, S-Z. Luo and W-G. Song, *Chem. Commun.*, 2010, **46**, 1109.

30. L. Zhao, Z.-Z. Sun and J. Ma, *Environ. Sci. Technol.*, 2009, **43**, 4157; (b) J. C. McKeen, Y. S. Yan and M. E. Davis, *Chem. Mater.*, 2008, **20**, 3791.

31. A. Bassan, W. Zou, E. Reyes, F. Himo and A. Cordova, *Angew. Chem. Int. Ed.*, 2005, **44**, 7028.

32. F. Alonso, P. Riente, J. A. Sirvent and M. Yus, *Appl. Catal. A: Gen.*, 2010, **378**, 42.

33. X-H. Chen, J. Yu and L-Z. Gong, *Chem. Commun.*, 2010, **46**, 6437.

(Spectral Data)

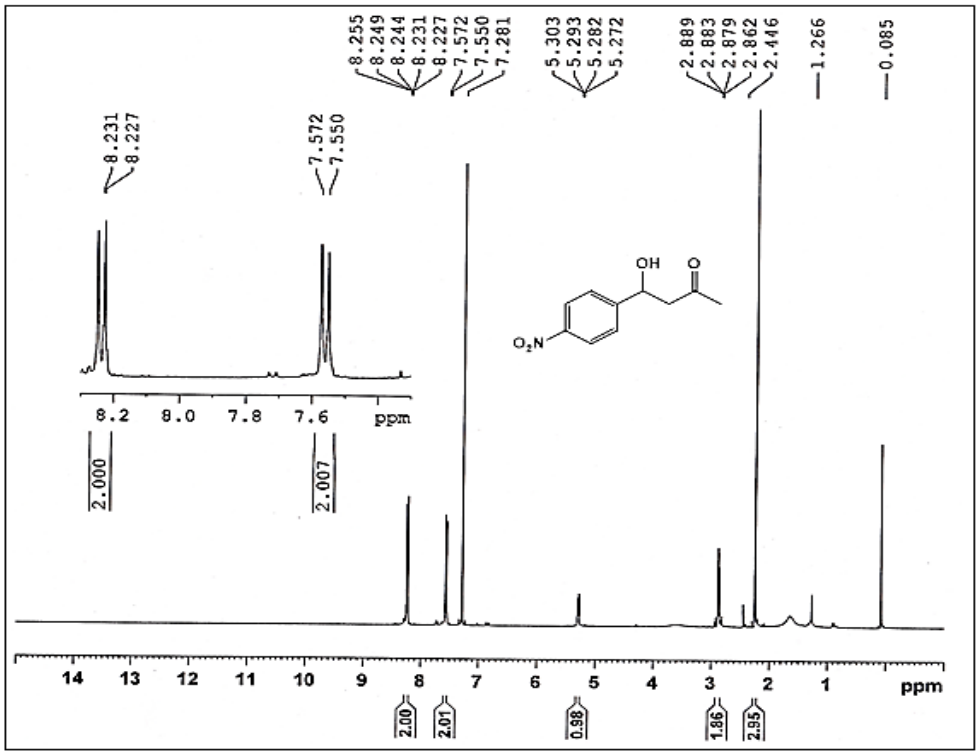

Figure S1 [1]HNMR spectra of 4-Hydroxy-4-(4'-nitrophenyl)butan-2-one

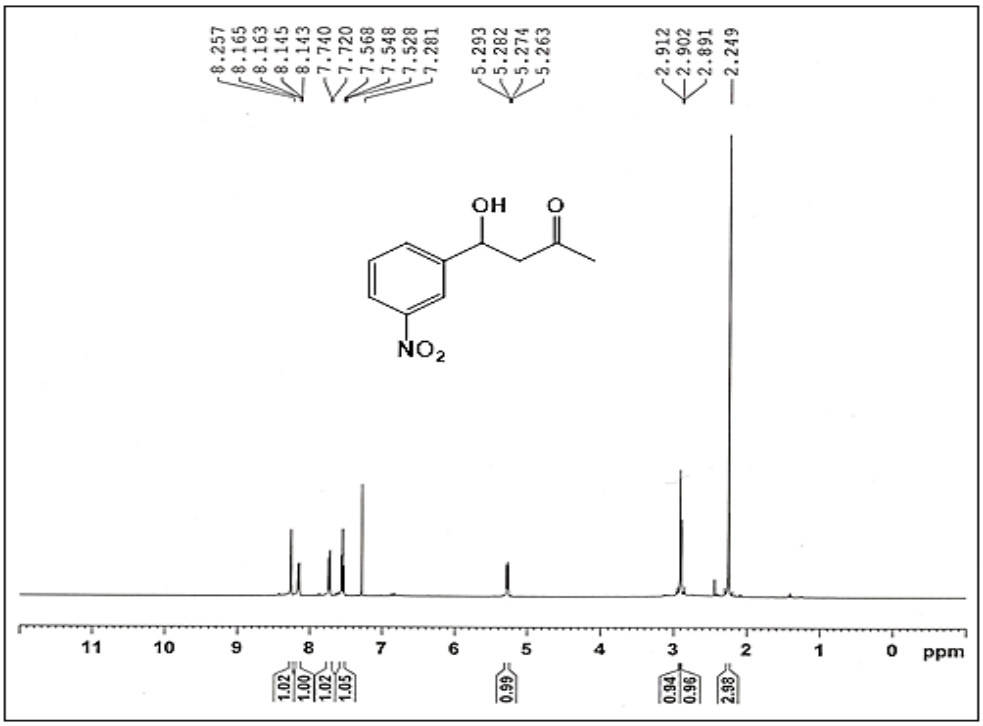

Figure S2 [1]HNMR spectra of 4-Hydroxy-4-(3'-nitrophenyl)butan-2-one

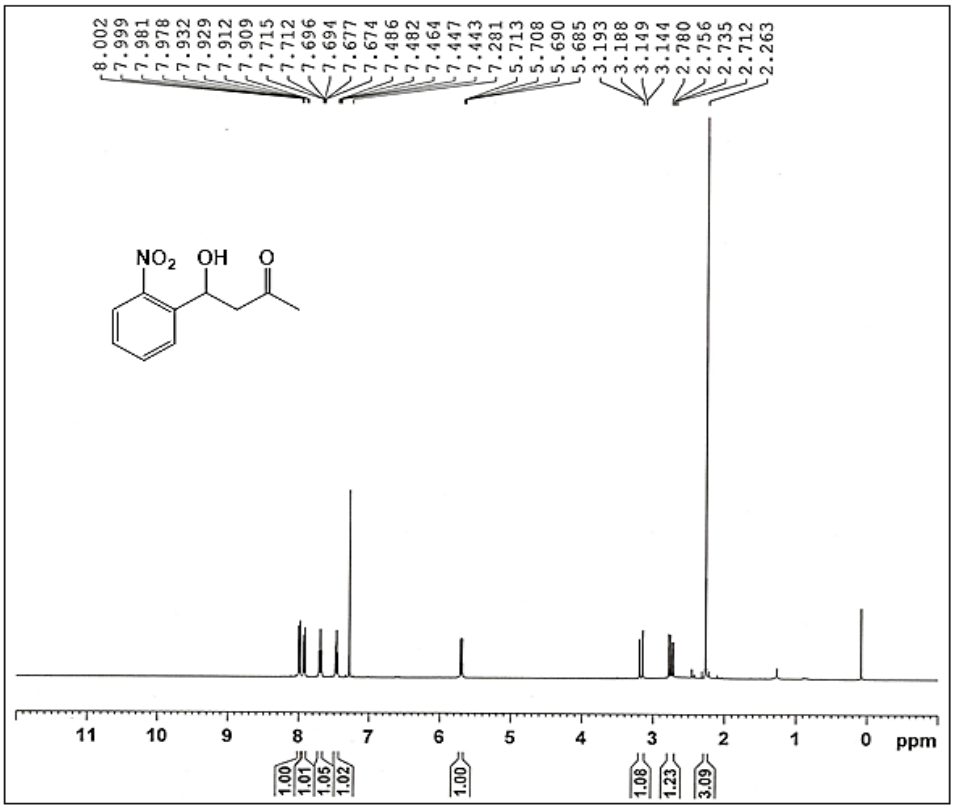

Figure S3 [1]HNMR spectra of 4-Hydroxy-4-(2'-nitrophenyl)butan-2-one

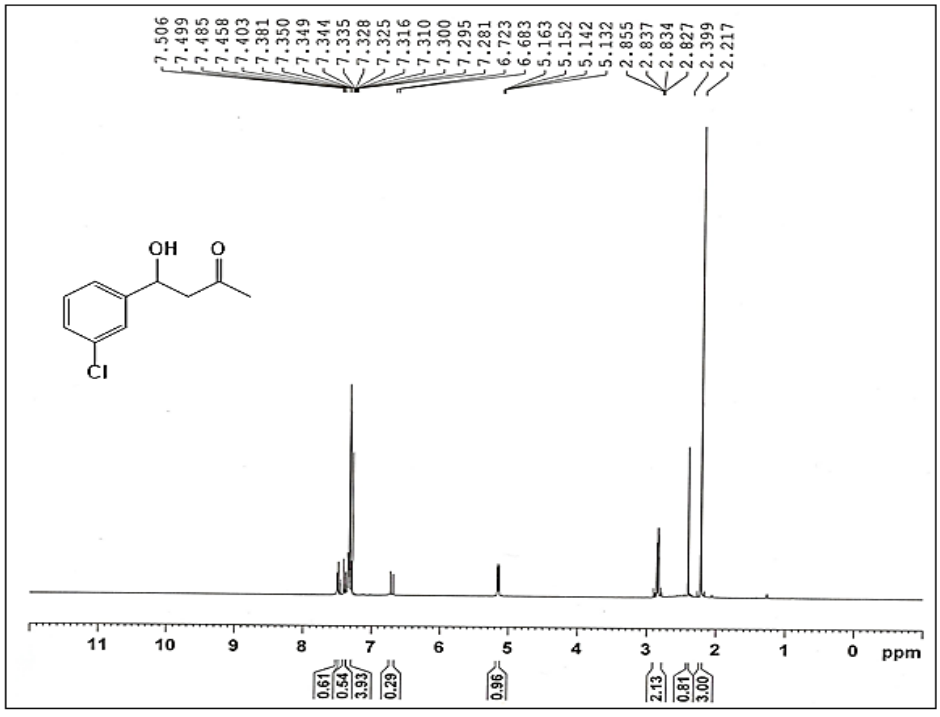

Figure S4 [1]HNMR spectra of 4-Hydroxy-4-(3'-chlorophenyl)butan-2-one

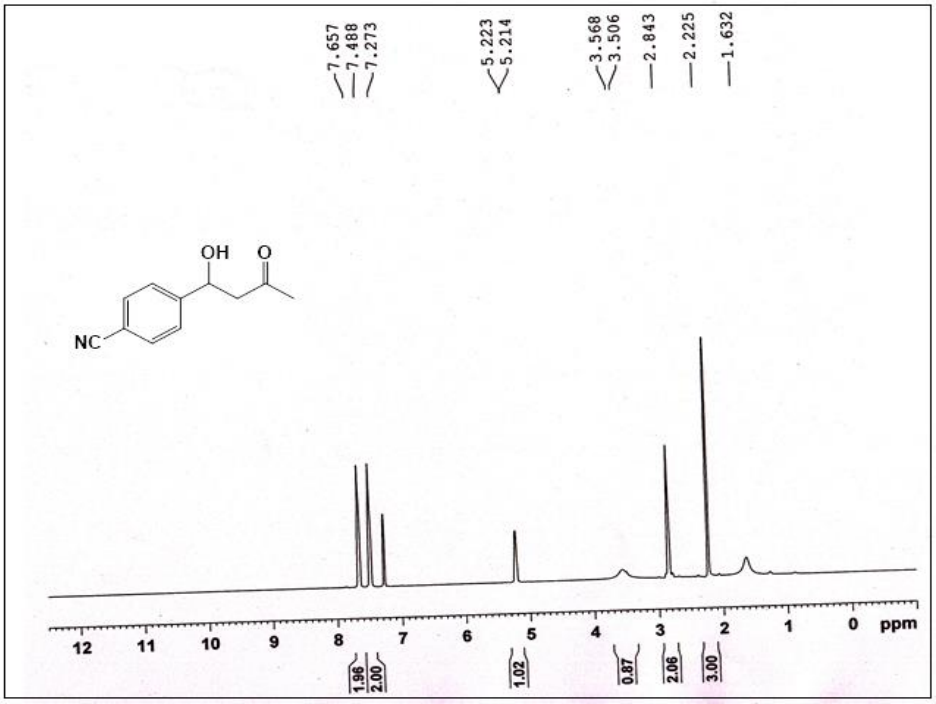

Figure S5 [1]HNMR spectra of 4-Hydroxy-4-(4'-cyanophenyl)butan-2-one

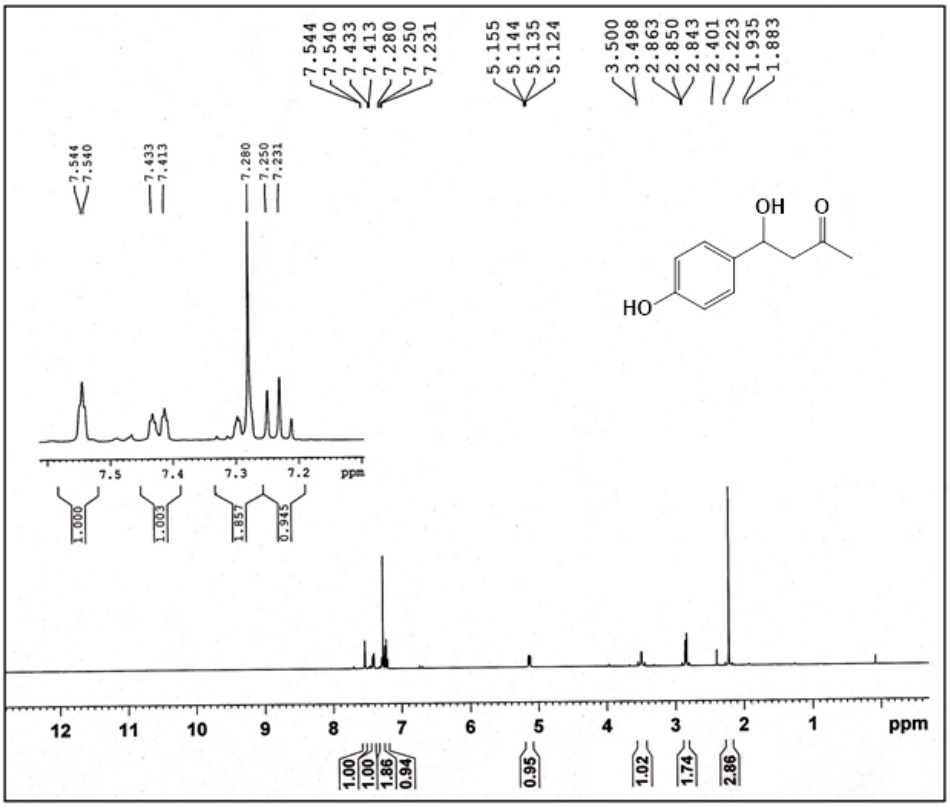

Figure S6 [1]HNMR spectra of 4-Hydroxy-4-(4'-hydroxyphenyl)butan-2-one

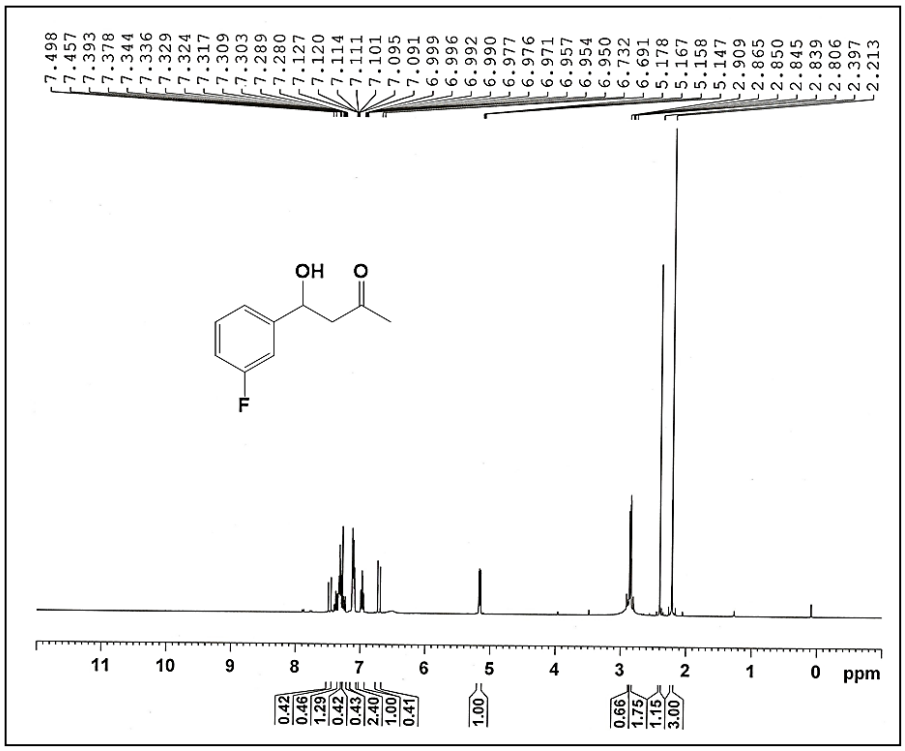

Figure S7 1HNMR spectra of 4-Hydroxy-4-(3'-florophenyl)butan-2-one

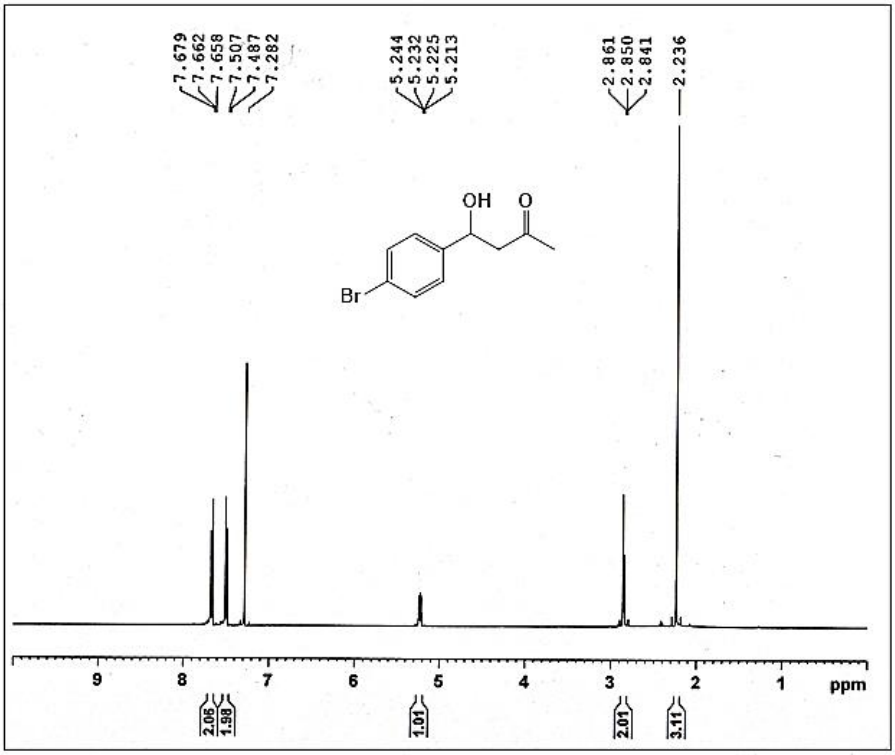

Figure S8 [1]HNMR spectra of 4-Hydroxy-4-(4'-bromophenyl)butan-2-one

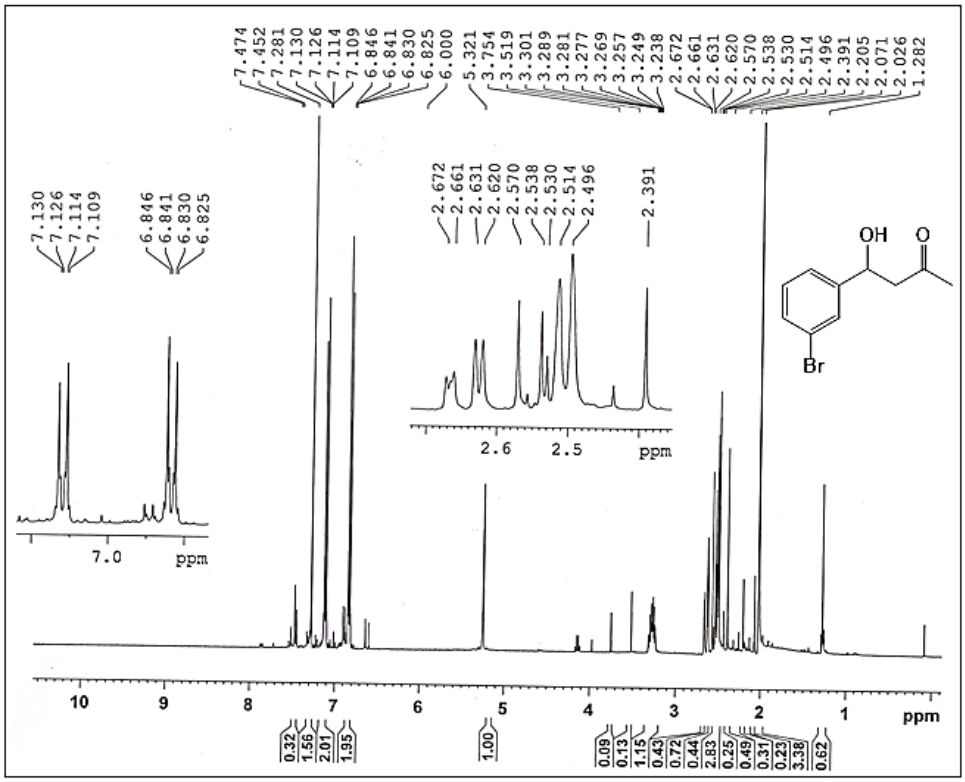

Figure S9 [1]HNMR spectra of 4-Hydroxy-4-(3'-bromophenyl)butan-2-one